Pygmy and giant dipole resonances in neutron-rich nuclei within the quasiparticle representation of the phonon damping model

Nguyen Dinh Dang,[1,*] Vuong Kim Au,[1,†] Toshio Suzuki,[2,‡] and Akito Arima[1,3,§]
[1]*RI-Beam Factory Project Office, RIKEN, 2-1 Hirosawa, Wako, Saitama 351-0198, Japan*
[2]*Department of Physics, College of Humanities and Sciences, Nihon University, Sakurajosui 3-25-40, Setagaya-ku, Tokyo 156-8550, Japan*
[3]*House of Councillors, Nagata-cho 2-1-1, Chiyoda-ku, Tokyo 100-8962, Japan*
(Received 5 October 2000; published 1 March 2001)

The quasiparticle representation of the phonon damping model (PDM) is developed to include the superfluid pairing correlations microscopically. The formalism is applied to calculate the photoabsorption and the electromagnetic (EM) differential cross sections of $E1$ excitations in neutron-rich oxygen and calcium isotopes. The calculated photoabsorption cross sections agree reasonably well with the available data for ^{16,18}O and ^{40,48}Ca. The fractions of energy-weighted sum of strength in the region of the pygmy dipole resonance (PDR) ($E_\gamma \leqslant 15-16$ MeV) and the PDR peaks in the EM cross sections for ^{20,22}O are also found in reasonable agreement with experimental systematics. The deviation from the prediction given by the cluster model's sum rule shows the importance of the effect of coupling to noncollective degrees of freedom in the damping of pygmy and giant dipole resonances.

DOI: 10.1103/PhysRevC.63.044302 PACS number(s): 21.10.Pc, 24.30.Cz, 21.60.−n, 25.20.−x

I. INTRODUCTION

Recent years have seen intensive studies of effects due to varying the ratio of proton Z and neutron N numbers on different nuclear structure characteristics as nuclei deviate from their valley of β stability. One of the phenomena is the pygmy dipole resonance (PDR) in neutron-rich nuclei or soft dipole mode in neutron halo nuclei. The PDR leads to the enhancement of dipole strength below the region of the usual giant dipole resonance (GDR). The PDR, by itself, is not a new subject as it was observed experimentally in photonuclear reactions in ^{18}O more than two decades ago [1]. The renewed interest in this phenomenon arises mainly due to the prospects of using radioactive-isotope (RI) beams to study unstable nuclei. With the recent method of utilizing the electromagnetic (EM) excitation process at high energies the $E1$ strength distribution can be studied up to the region of GDR in light neutron-rich isotopes [2].

One of the challenges in the theoretical study of exotic nuclei is how to go from the valley of β stability, where predictions given by various models for major fundamental nuclear properties are similar, to the region of nuclei with extreme N/Z ratios, where theoretical predictions become quite model dependent. The PDR was predicted by several theoretical models starting from an application of the cluster model (CM) [3], where the low-lying dipole mode is described as a result of oscillation of neutron excess against the core, the Skyrme-Hartree-Fock model (SHF) [4], the Hartree-Fock plus random-phase approximation (HF-RPA) model [5], to the large-scale shell-model calculations (LSSM) [6]. The LSSM uses an interaction, which is determined as a least-square fit of the particle-hole (p-h) two-body matrix elements to the binding and excitation energies of nuclei with mass number $A=10-20$. The width of the GDR was not explicitly calculated in these theoretical studies. Instead, it was introduced as a width parameter from the Gaussian [4] or Breit-Wigner [5,6] distribution. The recent preliminary experimental results at GSI [2] have shown that the energy-weighted sum (EWS) of the PDR strength does not follow the prediction of the CM. The prediction given by LSSM agrees qualitatively with the preliminary data for the EM cross sections of the PDR in ^{20,22}O [2], but the GDR shapes given by LSSM disagree with the well-established experimental systematics for photonuclear reaction cross sections in ^{16,18}O [1]. Given the rather scarce experimental data on GDR and PDR in neutron-rich nuclei at present, it is desirable to have an extension toward the region with $N \gg Z$ based on a theoretical model, which includes properly the damping mechanism and describes satisfactorily the well-known systematics of GDR shapes in β-stable nuclei.

Recently we made an attempt to develop such an approach in [7], where the phonon damping model (PDM) [8] was applied to study damping of the GDR in neutron-rich nuclei. The GDR width is calculated explicitly within the PDM via coupling of the GDR phonon to p-h configurations (at zero temperature). However, the superfluid pairing correlations, which are quite important for low-lying states in neutron-rich open-shell nuclei, were neglected. Instead, the matrix elements between the levels close to the Fermi surface in neutron-rich nuclei were increased in an ad hoc manner to simulate the strong coupling between them. In this way the low-lying dipole mode was obtained qualitatively. This result encourages us to elaborate the PDM further toward a microscopic description of damping of the GDR in

*On leave of absence from the Institute of Nuclear Science and Technique, VAEC, Hanoi, Vietnam. Electronic address: dang@rikaxp.riken.go.jp
†Present address: Texas A&M University, College Station, TX 77840-3366
‡Electronic address: suzuki@chs.nihon-u.ac.jp
§Electronic address: akito_arima@sangiin.go.jp

neutron-rich nuclei. The aim of the present paper is to include microscopically the superfluid pairing correlations in the PDM using the quasiparticle representation, and apply the formalism to calculate the photoabsorption and EM cross sections in neutron-rich oxygen and calcium isotopes. The paper is organized as follows. The formalism of the model is developed in Sec. II. The results of numerical calculations are discussed in Sec. III in comparison with available experimental data whenever possible. The paper is summarized in the last section where conclusions are drawn.

II. QUASIPARTICLE REPRESENTATION OF THE PHONON DAMPING MODEL

The quasiparticle representation of the PDM Hamiltonian [8,9] is obtained by adding the superfluid pairing interaction in it and expressing the particle (p) and hole (h) creation and destruction operators, $a_s^\dagger$ and a_s ($s=p,h$), in terms of the quasiparticle operators, $\alpha_s^\dagger$ and α_s, using the Bogolyubov canonical transformation. As a result, the PDM Hamiltonian for the description of $E\lambda$ excitations can be written in a spherical basis as

$$H=\sum_{jm}\epsilon_j\alpha_{jm}^\dagger\alpha_{jm}+\sum_{\lambda\mu i}\omega_{\lambda i}b_{\lambda\mu i}^\dagger b_{\lambda\mu i}+\frac{1}{2}\sum_{\lambda\mu i}\frac{(-1)^{\lambda-\mu}}{\hat{\lambda}}\sum_{jj'}f_{jj'}^{(\lambda)}\{u_{jj'}^{(+)}[A_{jj'}^\dagger(\lambda\mu)+A_{jj'}(\lambda\tilde{\mu})]+v_{jj'}^{(-)}[B_{jj'}^\dagger(\lambda\mu)+B_{jj'}(\lambda\tilde{\mu})]\}(b_{\lambda\mu i}^\dagger+b_{\lambda\tilde{\mu}i}), \quad (1)$$

where $\hat{\lambda}=\sqrt{2\lambda+1}$. The first term on the right-hand side (RHS) of Hamiltonian (1) corresponds to the independent-quasiparticle field. The second term stands for the phonon field described by phonon operators, $b_{\lambda\mu i}^\dagger$ and $b_{\lambda\mu i}$, with multipolarity λ, which generate the harmonic collective vibrations such as the GDR. Phonons are ideal bosons within the PDM, i.e., they have no fermion structure. The last term is the coupling between quasiparticle and phonon fields, which is responsible for the microscopic damping of collective excitations.

In Eq. (1) the following standard notations are used:

$$A_{jj'}^\dagger(\lambda\mu)=\sum_{mm'}\langle jmj'm'|\lambda\mu\rangle\alpha_{jm}^\dagger\alpha_{j'm'}^\dagger,$$

$$B_{jj'}^\dagger(\lambda\mu)=-\sum_{mm'}(-1)^{j'-m'}\langle jmj'-m'|\lambda\mu\rangle\alpha_{jm}^\dagger\alpha_{j'm'}, \quad (2)$$

with $(\lambda\tilde{\mu})\leftrightarrow(-1)^{\lambda-\mu}(\lambda-\mu)$. Functions $u_{jj'}^{(+)}\equiv u_jv_{j'}+v_ju_{j'}$ and $v_{jj'}^{(-)}\equiv u_ju_{j'}-v_jv_{j'}$ are combinations of Bogolyubov's u and v coefficients. The quasiparticle energy ϵ_j is calculated from the single-particle energy E_j as

$$\epsilon_j=\sqrt{(\tilde{E}_j-E_F)^2+\Delta^2},\quad \tilde{E}_j\equiv E_j-Gv_j^2, \quad (3)$$

where the pairing gap Δ and the Fermi energy E_F are defined as solutions of the BCS equations (see, e.g., [10])

$$\sum_j(j+\tfrac{1}{2})\frac{1-2n_j}{\epsilon_j}=\frac{2}{G}, \quad (4)$$

$$\sum_j(j+\tfrac{1}{2})\left[1-\frac{\tilde{E}_j-E_F}{\epsilon_j}(1-2n_j)\right]=N, \quad (5)$$

with N and G being the neutron (or proton) number and pairing constant, respectively. The quantity $n_j=\langle\alpha_j^\dagger\alpha_j\rangle$ is the quasiparticle occupation number defined within the grand canonical ensemble at a given temperature T. It becomes zero at $T=0$. Another way of approaching the BCS equations (4) and (5) is to define the pairing constant G and the Fermi energy E_F at a given value of Δ (e.g., using the approximate systematic for the pairing gap $\Delta\simeq 12/\sqrt{A}$ [11]). The operators in Eq. (2) and their Hermitian conjugates satisfy the following commutation relations within the ensemble average:

$$\langle[A_{jj'}(\lambda\mu),A_{j_1j_1'}^\dagger(\lambda'\mu')]\rangle=(1-n_j-n_{j'})\delta_{\lambda\lambda'}\delta_{\mu\mu'}\times[\delta_{jj_1}\delta_{j'j_1'}+(-1)^{j'-j+\lambda}\delta_{jj_1'}\delta_{j'j_1}], \quad (6)$$

$$\langle[B_{jj'}(\lambda\mu),B_{j_1j_1'}^\dagger(\lambda'\mu')]\rangle=(n_{j'}-n_j)\delta_{\lambda\lambda'}\delta_{\mu\mu'}\delta_{jj_1}\delta_{j'j_1'}, \quad (7)$$

where it is assumed that $\langle\alpha_j^\dagger\alpha_{j'}\rangle=0$ if $j\neq j'$.

The equation for the propagation of the GDR phonon, which is damped due to coupling to the quasiparticle field, is derived below, making use of the double-time Green's function method [12]. For this purpose, the following double-time Green's functions are introduced similar to the case without pairing within the PDM [8]. They are (i) the phonon propagation, $G_{\lambda i}(t-t')=\langle\langle b_{\lambda\tilde{\mu}i}(t);b_{\lambda\mu i}^\dagger(t')\rangle\rangle$, (ii) the forward-going transition between quasiparticle pair and phonon, $\mathcal{G}^A_{jj';\lambda i}(t-t')=\langle\langle A_{jj'}(\lambda\tilde{\mu})(t);b_{\lambda\mu i}^\dagger(t')\rangle\rangle$, (iii) the backward-going transition between quasiparticle pair and phonon, $\mathcal{G}^{A^\dagger}_{jj';\lambda i}(t-t')=\langle\langle A_{jj'}^\dagger(\lambda\mu)(t);b_{\lambda\mu i}^\dagger(t')\rangle\rangle$, (iv) the forward-going transition between scattering-quasiparticle pair and phonon, $\mathcal{G}^B_{jj';\lambda i}(t-t')=\langle\langle B_{jj'}(\lambda\tilde{\mu})(t);b_{\lambda\mu i}^\dagger(t')\rangle\rangle$, and (v) the backward-going transition between the scattering-quasiparticle pair and phonon, $\mathcal{G}^{B^\dagger}_{jj';\lambda i}(t-t')=\langle\langle B_{jj'}^\dagger(\lambda\mu)(t);b_{\lambda\mu i}^\dagger(t')\rangle\rangle$. Here the conventional notation of the double-time Green's functions [12] is used. Following the standard procedure of deriving the equation for the double-time Green's function with respect to the Hamiltonian (1), and using of the commutation relations (6) and (7), one obtains a closed set of equations for these Green's functions, whose Fourier transform into the energy plane E is

$$(E-\omega_{\lambda i})G_{\lambda i}(E)-\frac{1}{2\hat{\lambda}}\sum_{jj'} f^{(\lambda)}_{jj'}\{u^{(+)}_{jj'}[\mathcal{G}^{A}_{jj';\lambda i}(E)+\mathcal{G}^{A^\dagger}_{jj';\lambda i}(E)] + v^{(-)}_{jj'}[\mathcal{G}^{B}_{jj';\lambda i}(E)+\mathcal{G}^{B^\dagger}_{jj';\lambda i}(E)]\}=\frac{1}{2\pi}, \tag{8}$$

$$(E-\epsilon_j-\epsilon_{j'})\mathcal{G}^{A}_{jj';\lambda i}(E)-\frac{1}{\hat{\lambda}}f^{(\lambda)}_{jj'}u^{(+)}_{jj'}(1-n_j-n_{j'})G_{\lambda i}(E)=0, \tag{9}$$

$$(E+\epsilon_j+\epsilon_{j'})\mathcal{G}^{A^\dagger}_{jj';\lambda i}(E)+\frac{1}{\hat{\lambda}}f^{(\lambda)}_{jj'}u^{(+)}_{jj'}(1-n_j-n_{j'})G_{\lambda i}(E)=0, \tag{10}$$

$$(E-\epsilon_j+\epsilon_{j'})\mathcal{G}^{B}_{jj';\lambda i}(E)+\frac{1}{\hat{\lambda}}f^{(\lambda)}_{jj'}v^{(-)}_{jj'}(n_j-n_{j'})G_{\lambda i}(E)=0, \tag{11}$$

$$(E+\epsilon_j-\epsilon_{j'})\mathcal{G}^{B^\dagger}_{jj';\lambda i}(E)-\frac{1}{\hat{\lambda}}f^{(\lambda)}_{jj'}v^{(-)}_{jj'}(n_j-n_{j'})G_{\lambda i}(E)=0. \tag{12}$$

Substituting $\mathcal{G}^{A}_{jj';\lambda i}(E)$, $\mathcal{G}^{A^\dagger}_{jj';\lambda i}(E)$, $\mathcal{G}^{B}_{jj';\lambda i}(E)$, and $\mathcal{G}^{B^\dagger}_{jj';\lambda i}(E)$ at the left-hand side (LHS) for Eq. (8) with their expressions in terms of $G_{\lambda i}(E)$ from Eqs. (9)–(12), we obtain the equation for the Green's function of phonon propagation $G_{\lambda i}(E)$ in the form

$$G_{\lambda i}(E)=\frac{1}{2\pi}\frac{1}{E-\omega_{\lambda i}-P_{\lambda i}(E)}, \tag{13}$$

where the explicit form of the polarization operator $P_{\lambda i}(E)$ is

$$P_{\lambda i}(E)=\frac{1}{\hat{\lambda}^2}\sum_{jj'}[f^{(\lambda)}_{jj'}]^2\left[\frac{(u^{(+)}_{jj'})^2(1-n_j-n_{j'})(\epsilon_j+\epsilon_{j'})}{E^2-(\epsilon_j+\epsilon_{j'})^2} - \frac{(v^{(-)}_{jj'})^2(n_j-n_{j'})(\epsilon_j-\epsilon_{j'})}{E^2-(\epsilon_j-\epsilon_{j'})^2}\right]. \tag{14}$$

The phonon damping $\gamma_{\lambda i}(\omega)$ (ω real) is obtained as the imaginary part of the analytic continuation of the polarization operator $P_{\lambda i}(E)$ into the complex energy plane $E=\omega \pm i\varepsilon$. Its final form is

$$\gamma_{\lambda i}(\omega)=\frac{\pi}{2\hat{\lambda}^2}\sum_{jj'}[f^{(\lambda)}_{jj'}]^2\{(u^{(+)}_{jj'})^2(1-n_j-n_{j'}) \times[\delta(E-\epsilon_j-\epsilon_{j'})-\delta(E+\epsilon_j+\epsilon_{j'})] -(v^{(-)}_{jj'})^2(n_j-n_{j'})[\delta(E-\epsilon_j+\epsilon_{j'}) -\delta(E+\epsilon_j-\epsilon_{j'})]\}. \tag{15}$$

At zero temperature all the quasiparticle occupation numbers n_j are zero, so the factor $1-n_j-n_{j'}$ becomes 1, while the last terms at the RHS of Eqs. (14) and (15), which contain $(v^{(-)}_{jj'})^2$, vanish. It is also worth noticing that the contribution to the GDR of the term $\sim\delta(E+\epsilon_j+\epsilon_{j'})$ due to the backward-going process should be negligible as its maximum is at $-(\epsilon_j+\epsilon_{j'})<0$.

The energy ω of giant resonance (damped collective phonon) is found as the pole of the Green's function (13), i.e., as the solution of the following equation:

$$\bar{\omega}-\omega_{\lambda i}-P_{\lambda i}(\bar{\omega})=0. \tag{16}$$

The width Γ_λ of giant resonance is calculated as twice of the damping $\gamma_\lambda(\omega)$ at $\omega=\bar{\omega}$, i.e.,

$$\Gamma_\lambda=2\gamma_\lambda(\bar{\omega}), \tag{17}$$

where $\lambda=1$ corresponds to the GDR. As has been discussed previously [8,9], the presence of the polarization operator (14) due to p-h–phonon coupling in the last term of the RHS of Hamiltonian (1) and the property of the double-time Green's function, which allows the analytic continuation into the complex energy plan, allows the damping to be calculated in an explicit and microscopic way given by Eq. (15). The PDM-1 [8], used in the present work, includes only lowest-onder graphs explicitly in the p-h–phonon coupling, while the contribution of higher-order graphs is effectively included in the p-h–phonon coupling parameter f_1 (see the next section). The PDM-2 includes explicitly the coupling to all higher-order graphs up to two-phonon ones (see the detailed discussion in [9]). This shows that the damping within the PDM, even in its simplest version PDM-1, is not the Landau damping. The latter is the deviation from the centroid of a group of closely located harmonic oscillators, provided coupling to continuum is neglected. These harmonic oscillators can be found as solutions of the RPA equation. Each of them can be put in one-to-one correspondence with an undamped phonon with energy $\omega_{\lambda i}$ within the PDM [before the coupling caused by the last term at the RHS of Eq. (1) is switched on]. Since there is no coupling of these modes to the quasiparticle (or single-particle) field within the RPA, all the solutions of the RPA are located on the real axis, and there is no imaginary part that corresponds to absorption (damping) within the RPA due to coupling to noncollective p-h configurations or higher ones as in the PDM. A smearing parameter, which is sometimes introduced in the RPA, is only to transform a discrete strength distribution to a continuous one.

The line shape of the GDR is described by the strength function $S_{\rm GDR}(\omega)$, which is derived from the spectral intensity in the standard way using the analytic continuation of the Green function (13) [13] and by expanding the polarization operator (14) around $\bar{\omega}$ [12]. The final form of $S_{\rm GDR}(\omega)$ is [8]

$$S_{\rm GDR}(\omega)=\frac{1}{\pi}\frac{\gamma_{\rm GDR}(\omega)}{(\omega-\bar{\omega})^2+\gamma^2_{\rm GDR}(\omega)}. \tag{18}$$

Note that function (18) has only a Breit-Wigner-like form since the damping $\gamma_{\mathrm{GDR}}(\omega)$ depends on the energy ω. The photoabsorption cross section $\sigma(E_\gamma)$ is calculated from the strength function $S_{\mathrm{GDR}}(E_\gamma)$ as

$$\sigma(E_\gamma)=c_1 S_{\mathrm{GDR}}(E_\gamma)E_\gamma, \tag{19}$$

where $E_\gamma \equiv \omega$ is used to denote the energy of γ emission. The normalization factor c_1 is defined so that the total integrated photoabsorption cross section $\sigma=\int\sigma(E_\gamma)dE_\gamma$ satisfies the GDR sum rule $\mathrm{SR}_{\mathrm{GDR}}$; hence

$$c_1=\mathrm{SR}_{\mathrm{GDR}}\Big/\int_0^{E_{\max}} S_{\mathrm{GDR}}(E_\gamma)E_\gamma dE_\gamma. \tag{20}$$

In heavy nuclei with $A\geqslant 40$, the GDR exhausts the Thomas-Reich-Kuhn (TRK) sum rule $\mathrm{SR}_{\mathrm{GDR}}=\mathrm{TRK}\equiv 60NZ/A$ MeV mb at the upper integration limit $E_{\max}\simeq 30$ MeV, and exceeds TRK ($\mathrm{SR}_{\mathrm{GDR}}>\mathrm{TRK}$) at $E_{\max}>30$ MeV due to the contribution of exchange forces. In some light nuclei, such as ^{16}O, the observed photoabsorption cross section exhausts only around 60% of TRK up to $E_{\max}\simeq 30$ MeV [1].

According to [14,15], the EM cross section σ_{EM} is calculated from the corresponding photoabsorption cross section $\sigma(E_\gamma)$ and the photon spectral function $N(E_\gamma)$ as

$$\sigma_{\mathrm{EM}}\equiv\int\frac{d\sigma_{\mathrm{EM}}}{dE_\gamma}dE_\gamma=\int N(E_\gamma)\sigma(E_\gamma)dE_\gamma,$$

$$N(E_\gamma)=2\pi\int_{b_{\min}}^{\infty} e^{-m(b)}N(E_\gamma,b)b\,db. \tag{21}$$

The expression for the spectrum $N(E_\gamma,b)$ of a virtual photon from a stationary target as seen by a projectile moving with a velocity $\beta=v/c$ at impact parameter b is also given in [15]. The mean number of photons absorbed by the projectile is calculated as $m(b)=\int_{E_{\min}}^{\infty}N(E_\gamma,b)\sigma(E_\gamma)dE_\gamma$.

III. NUMERICAL RESULTS

The calculations of photoabsorption and EM cross sections have been carried out for oxygen isotopes with $A=16$, 18, 20, 22, and 24 and for calcium isotopes with $A=40$, 42, 44, 46, 48, 50, 52, and 60. The calculations employ the spherical-basis single-particle energies E_j obtained within the Hartree-Fock method using the Skyrme-type SGII interaction [16]. They span a large space of 36 proton and 36 neutron discrete levels from $E_j\simeq -43$ to -36 MeV up to $E_j\simeq 76$ to 90 MeV for $^{16,20-24}$O. The number of neutron levels for ^{18}O is 42. For calcium isotopes, the single-particle levels used in calculations are between around -46 MeV and 51 MeV. The number of proton levels is 48, while the number of neutron levels is 97 for $^{40-52}$Ca and 103 for ^{60}Ca. The principal point, which is maintained throughout our study of the GDR in neutron-rich nuclei, is that we extrapolate the description of closed-shell nuclei within PDM to the region of neutron open-shell nuclei, assuming they are all spherical. This means that the two PDM parameters ω_λ ($\lambda=1$) and $f_1=f_{jj'}^{(1)}$ for all p-h indices ($j=p, j'=h$) are chosen so that the values of GDR energy $E_{\mathrm{GDR}}\equiv\overline{\omega}$ and width Γ_{GDR}, calculated from Eqs. (16) and (17) for ^{16}O and ^{40,48}Ca, reproduce their corresponding experimental values $E_{\mathrm{GDR}}^{\mathrm{expt}}$ and $\Gamma_{\mathrm{GDR}}^{\mathrm{expt}}$ (see [8] for more details about the procedure of choosing parameters within PDM). The values of PDM parameters for ^{16}O are then fixed in calculations for all oxygen isotopes ($N\geqslant Z$). For calcium isotopes, we used the parameters selected for ^{40}Ca in calculations for isotopes with $20\leqslant N<28$, and those selected for ^{48}Ca in calculations with $N\geqslant 28$. The neutron pairing gap Δ_n is adjusted around the general trend $12/\sqrt{A}$ of the observed pairing gaps in stable nuclei. The adjustment is necessary to keep the GDR energy remain nearly unchanged with increasing N as the values of parameters ω_1 and f_1 are kept fixed for three groups of isotopes $^{16-24}$O, $^{40-46}$Ca, and $^{48-60}$Ca separately. The existence of the neutron-superfluid pairing gap leads to the deviation of the neutron Fermi surface from the step function so that many neutron levels above (below) it become close to the proton-hole (-particle) levels. This makes the p-h interaction between protons (π) and neutrons (ν) also important, especially when the pairing gap is large, as it is the case of some oxygen isotopes. Therefore, in the present work, we choose the PDM parameters and carry out the calculations with the sums in Eqs. (1), (14), and (15) running over all indices (j,j') with $j=(p_\pi,p_\nu)$ and $j'=(h_\pi,h_\nu)$. For double closed-shell nuclei ^{16}O and ^{40,48}Ca, where the pairing gap is zero, such a kind of enlargement of configuration space is compensated simply by a renormalization of f_1, which reduces its value by $\sim$25% for ^{16}O, and $\sim$35–37 % for ^{40,48}Ca, so that the GDR shape remains the same. For ^{16}O, we found the PDM parameters $\omega_1=22.5$ MeV and $f_1=0.6982$ MeV, which yield the GDR energy $E_{\mathrm{GDR}}=23.7$ MeV and width $\Gamma_{\mathrm{GDR}}=5.85$ MeV. For ^{40}Ca (^{48}Ca), the selected values of the PDM parameters are $\omega_1=19.51$ MeV and $f_1=0.3421$ MeV (0.4574 MeV), which lead to $E_{\mathrm{GDR}}=19.6$ MeV (19.4 MeV) and $\Gamma_{\mathrm{GDR}}=4.9$ MeV (7.15 MeV). Note that the parameter f_1 in the quasiparticle representation of the PDM is not the same as F_1 in [7]. The value of f_1 is also reduced because of a larger single-particle space (up to 90 MeV for oxygen isotopes, and 51 MeV for calcium isotopes) and the enlargement of the p-h configuration space discussed above. The selected values of Δ are plotted as black squares against the neutron number N in Fig. 1, which shows that they are within the range of experimental systematic for neutron pairing gaps in stable nuclei [11].

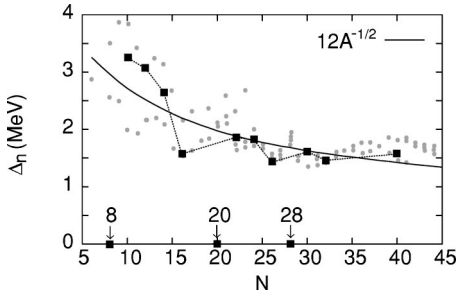

FIG. 1. Selected neutron pairing gaps Δ_n (black squares) in comparison with the experimental systematic for stable nuclei (gray circles) and the trend $\Delta=12/\sqrt{A}$ (solid line).

TABLE I. Energy E_{GDR} (in MeV), width Γ_{GDR} (in MeV) of GDR, and EWS of $E1$ strength (in units of TRK) up to 30 MeV [EWSS ($\leqslant$30)], and up to 100 MeV [EWSS ($\leqslant$50)], calculated within the PDM in oxygen and calcium isotopes. The available experimental energies and widths are shown in parentheses.

Nuclei	E_{GDR}	Γ_{GDR}	EWSS ($\leqslant$30)	EWSS ($\leqslant$50)
^{16}O	23.7 (23.2)	5.85	0.61 (0.54)	0.73
^{18}O	22.8 (23.7)	16.6	0.65	1.00 (0.91)
^{20}O	22.6	16.4	0.74	1.00
^{22}O	22.4	8.8	0.75	1.00
^{24}O	22.2	7.3	0.79	1.00
^{40}Ca	19.6 (19.7)	4.89 (5.0)	1.03	1.16
^{42}Ca	19.5	5.46	1.04	1.19
^{44}Ca	19.6	6.33	1.05	1.23
^{46}Ca	19.3	7.90	1.05	1.26
^{48}Ca	19.4 (19.5)	7.15 (6.98)	1.28	1.56
^{50}Ca	19.6	9.80	1.23	1.59
^{52}Ca	19.6	12.36	1.13	1.54
^{60}Ca	19.3	8.18	1.20	1.54

The δ function in the damping (15) is smoothed out using the representation $\delta(x)=[(x-i\varepsilon)^{-1}-(x+i\varepsilon)^{-1}]/(2\pi i)$ with $\varepsilon=0.5$–1 MeV. The averaged quantities such as the EWS of $E1$ strength and the shape of GDR do not change significantly using $0.1\leqslant\varepsilon\leqslant 1.5$ MeV. The results discussed below are obtained in calculations using the value of the smearing parameter ε equal to 0.5 MeV for oxygen isotopes, and 1 MeV for calcium isotopes. The normalization factor c_1 from Eq. (20) is defined as follows. For ^{16}O, the factor c_1 is chosen so that $\mathrm{SR}_{\mathrm{GDR}}$ reproduces the experimental EWS of $E1$ strength, which amounts to 54% of TRK with $E_{\max}=29$ MeV. For other oxygen isotopes, c_1 is found so that 100% of TRK is exhausted at $E_{\max}=50$ MeV. For calcium isotopes, c_1 is defined so that the EWS of $E1$ strength fulfills

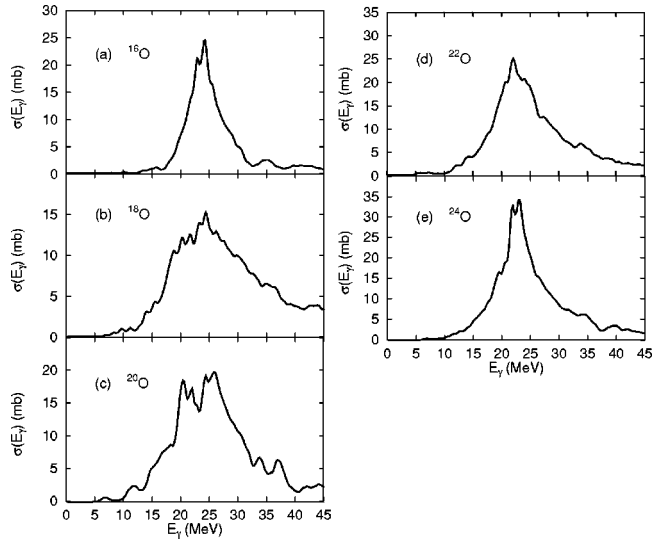

FIG. 2. Photoabsorption cross sections for oxygen isotopes obtained within the PDM.

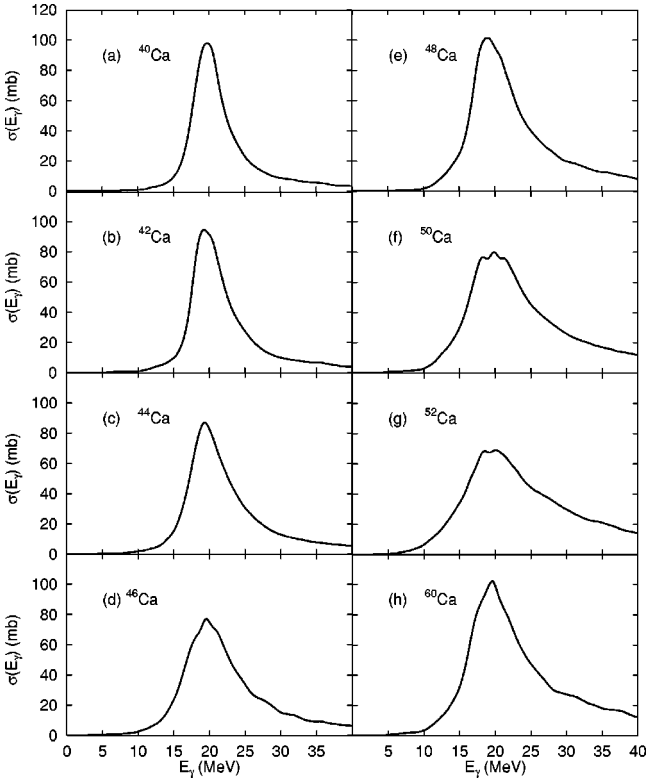

FIG. 3. Photoabsorption cross sections for calcium isotopes obtained within the PDM.

100% of TRK at $E_{\max}=28$ MeV for $40\leqslant A<48$, and 156 $\pm$3% of TRK at $E_{\max}=50$ MeV for $A\geqslant 48$. This criterion is an extrapolation of the experimental values of TRK fraction exhausted in the photoabsorption cross sections for ^{40,48}Ca. All the GDR parameters calculated within the PDM are shown in Table I.

Shown in Figs. 2 and 3 are the photoabsorption cross sections $\sigma(E_\gamma)$, which have been obtained within the PDM for oxygen and calcium isotopes, respectively. The shapes of the photoabsorption cross section calculated for stable isotopes ^{16,18}O and ^{40,48}Ca are found in overall reasonable agreement with available experimental data [1,17,18] as shown in the left panels of Fig. 4 [(a)–(d)]. This agreement is obviously better than those given by several elaborated models shown in the right panels of Fig. 4 [(e)–(h)], namely, the LSSM [6] using Warburton-Brown interaction WB10 [thin solid and thin dashed lines in panels (e) and (f) with $T_<=1$ and $T_>=2$ denoting two isospin components of the GDR in ^{18}O], the surface coupling model (SCM) using the coupling of p-h configurations with surface phonon [19] [dotted lines in panels (e) and (g)], the second RPA (SRPA) [20] [thick dashed line in panel (g)], and a microscopic model including $1p1h\oplus$phonon plus continuum (phPC) [21] [dash-dotted lines in panels (g) and (h)]. Experimental photoabsorption cross sections for other oxygen and calcium isotopes in the chains considered here are not available at present.

It is seen from Figs. 2 and 3 as well as from Table I that the GDR becomes broader for isotopes with $N>Z$. Its width is particularly large for isotopes between the double closed-

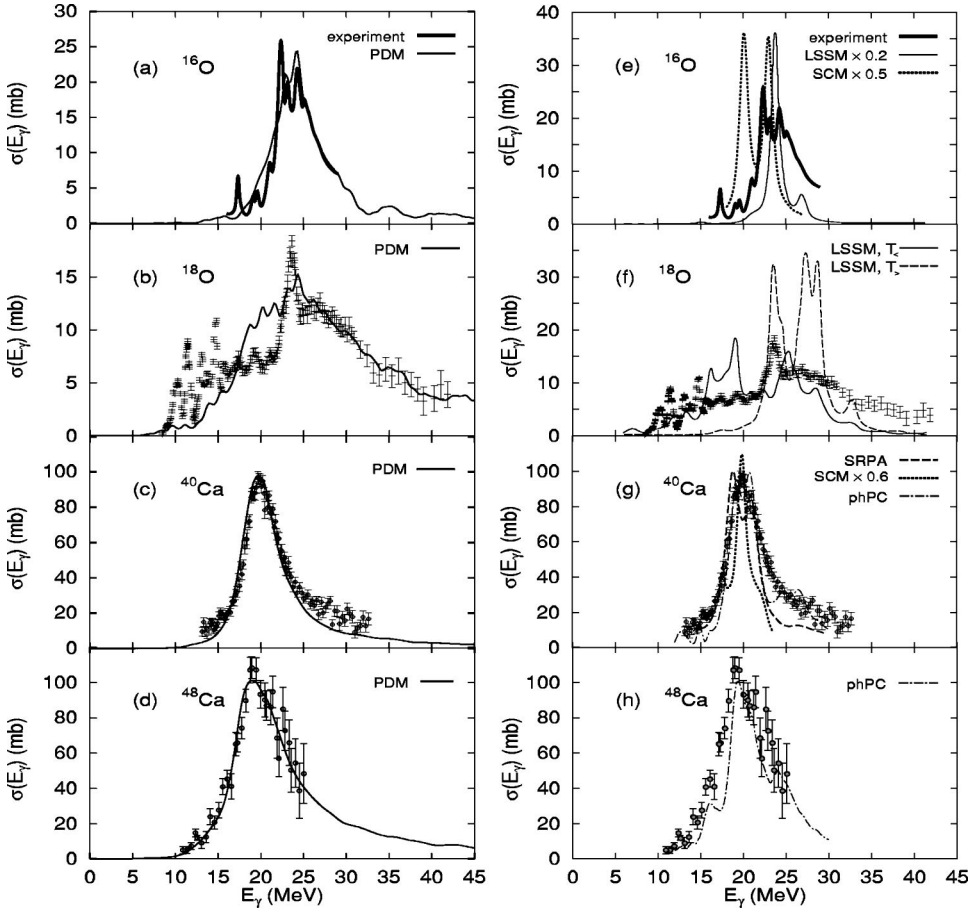

FIG. 4. Photoabsorption cross sections for ^{16,18}O and ^{40,48}Ca obtained within the PDM (left panels) and within other models mentioned in the text (right panels) in comparison with experimental data from [1] [thick solid line in (a) and (e)], [(b) and (f)], [17] [(c) and (g)], and [18] [(d) and (h)].

shell ones, such as ^{18,20}O or ^{52}Ca. The increase of GDR spreading enhances both of its low- and high-energy tails. In the region $E_\gamma \leqslant 15$ MeV, some weak structure of the PDR is visible for ^{18,20,22}O. In the rest of isotopes under study, except for an extension of the GDR tail toward lower energy, there is no visible structure of the PDR. This is in contrast with the results by some other approaches, where the GDR spreading width is not explicitly calculated, such as the SHF [4] or the LSSM [6]. In these approaches, prominent peaks in the GDR strength function are obtained in the region below 10–15 MeV in ^{20,22,24}O [4,6] and ^{60}Ca [4]. We note, however, that neither SHF nor LSSM can describe correctly the GDR shape in stable double-closed shell nuclei ^{16}O and ^{40,48}Ca.

The fractions of the EWS of strength exhausted by the low-energy tail of the GDR are shown in Figs. 5 and 6. The trend obtained within the PDM for oxygen isotopes reproduces the one observed in the recent experiments at the Darmstadt Heavy Ion Research Center GSI [2], which shows a clear deviation from the prediction by the cluster sum rule (CSR) (also called as molecular dipole sum rule) [3]. In calcium isotopes, where the GDR is more collective and exhausts 100% of TRK already below $E_\gamma = 30$ MeV, the prediction by CSR is fairly reproduced up to $A = 52$ using $E_{\max} = 16$ MeV. We notice that the fractions of EWS of PDR strength are not zero even for double closed-shell nuclei ^{16}O and ^{40,48}Ca because the low-energy tail in photoabsorption cross sections, which are experimentally observed and ob-

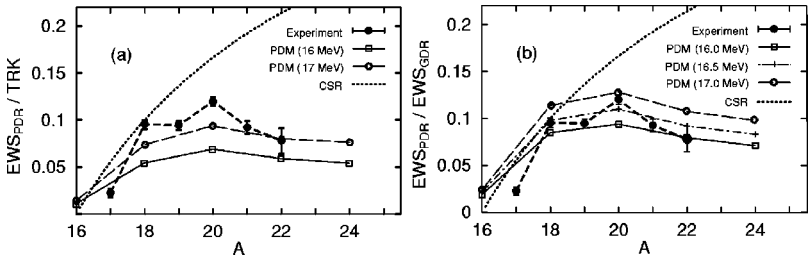

FIG. 5. EWS of PDR strength up to excitation energy $E_{\max}$ for oxygen isotopes. Results obtained within the PDM with $E_{\max} = 16$, 16.5, and 17 MeV are displayed as open boxes connected with a solid line, crosses connected with a dash-dotted line, and open circles connected with a thin dashed line, respectively. In (a) the PDM results are shown in units of TRK, while in (b) they are in units of the total GDR strength integrated up to 30 MeV. Experimental data (in units of TRK), obtained with $E_{\max} = 15$ MeV, are shown by full circles connected with a thick dashed line. The dotted line is the prediction by the cluster sum rule (CSR) (in units of TRK).

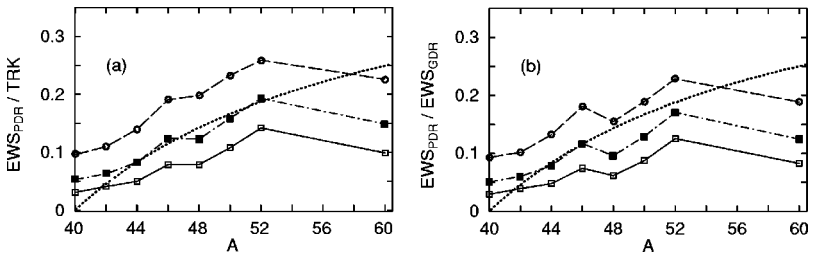

FIG. 6. EWS of PDR strength up to excitation energy $E_{\max}$ for calcium isotopes. Results obtained within the PDM with $E_{\max}=15$, 16, and 17 MeV are displayed as open boxes connected with a solid line, full boxes connected with a dash-dotted line, and open circles connected with a thin dashed line, respectively. Other notations are as in Fig. 5.

tained as results of calculations within the PDM, spreads below $E_\gamma=15$ MeV also for these nuclei. This is different from the prediction by the CM or LSSM, where these fractions are zero in closed-shell nuclei. The EWS of strength between 5 and 10 MeV obtained within PDM for ^{48}Ca is 0.52% of TRK to be compared with the value of (0.29 ± 0.04)% of TRK extracted in the recent high-photon scattering experiments [22]. The agreement between the PDM prediction and the experimental data for the photoabsorption cross sections as well as for the EWS of the PDR strength suggests that the mechanism of the damping of the PDR is dictated by the coupling between the GDR phonon and noncollective p-h excitations rather than by the oscillation of a collective neutron excess against the core. Strong pairing correlations also prevent the weakly bound neutrons from being decoupled from the rest of the system [23]. Only when the GDR is very collective so that it can be well separated from the neutron excess, does the picture of PDR damping become closer to the prediction by the CM.

The photon spectral function $N(E_\gamma)$ in the EM differential cross section $d\sigma_{\rm EM}/dE_\gamma$ [Eq. (21)] contains an exponentially decreasing factor $e^{-m(b)}$ with increasing E_γ. Its values for ^{22}O (on a ^{208}Pb target) are plotted as a function of E_γ in Fig. 7 at several projectile energies. It is clear that this behavior enhances the low-energy part of the $E1$ strength in the EM differential cross section. Therefore, the latter can be used as a magnifying glass for the structure of the PDR.

These cross sections obtained within the PDM are shown in Figs. 8 and 9 for oxygen and calcium isotopes, respectively. The calculations were carried out for a ^{208}Pb target at various projectile energies as shown in these figures. All the values shown in the figures have been normalized so that the integrated EM cross sections up to 50 MeV correspond to 100% of TRK. The PDR shows up in the EM cross sections of all neutron-rich isotopes, especially for ^{20,22}O, where a well-isolated peak located at around 7 MeV is clearly seen. The PDR becomes depleted when the neutron number approaches a magic number (where the GDR is most collective) as can be seen in calcium isotopes when N increases from 20 to 28. Therefore, the decrease of the PDR strength in ^{24}O and ^{60}Ca can be understood as the depletion on the way toward the next magic number ($N=28$ and 50, respectively). It is also important to point out the impact on the EM differential cross section by the behavior of the photon spectral function $N(E_\gamma)$ at various projectile energies. Indeed, because of the behavior of $N(E_\gamma)$ shown in Fig. 7, the decrease of the projectile energy from 700 MeV/nucleon to 300 MeV/nucleon strongly reduces the EM cross section in the GDR region (above 10 MeV), but leaves the PDR almost intact, as can be seen in Fig. 8. A further decrease of projectile energy to 50 MeV/nucleon suppresses completely the GDR peak and even enhances the PDR peak in some very neutron-rich nuclei ^{20,22,24}O or ^{52}Ca (dash-dotted lines in Figs. 8 and 9). This observation shows that, using high-intensity RI beams at low energies of around 50–60 MeV/nucleon, one may be able to observe a rather clean and sharp PDR peak in ^{20,22}O in the region around 7 MeV, and probably a broad peak below 5 MeV in ^{52}Ca.

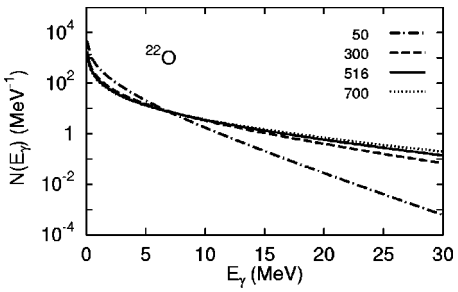

FIG. 7. Photon spectral function $N(E_\gamma)$ for ^{22}O as a function of E_γ. Different lines display results obtained at different projectile energies, whose values (in MeV/nucleon) are indicated in the figure.

The preliminary results of recent measurements of EM differential cross sections for $E1$ excitations in ^{20,22}O at GSI [2] have shown a peaklike structure at $E_\gamma \simeq 8$ MeV and another bump in the region between 12 and 16 MeV. Our results for the PDR from Figs. 8(c) and 8(d) are in qualitative agreement with the GSI data, which have been, however, presented with the detector response folded in. For a more quantitative comparison with the data, the EM cross sections calculated within the PDM must also be folded with the GSI instrumental response. Another difficulty for a direct comparison between the PDM results and the experimental ones is that the former are obtained from the total photoabsorption cross section, while only $1n$ up to $3n$ decay channels are included in the latter. Thus, the contribution from the one-proton decay channel, whose threshold is at around 19 MeV, is not included in the experimental data. Therefore, for a meaningful comparison between theory and experiment, a detailed simulation of the experimental response including γ detection is also needed, which is being planned [2].

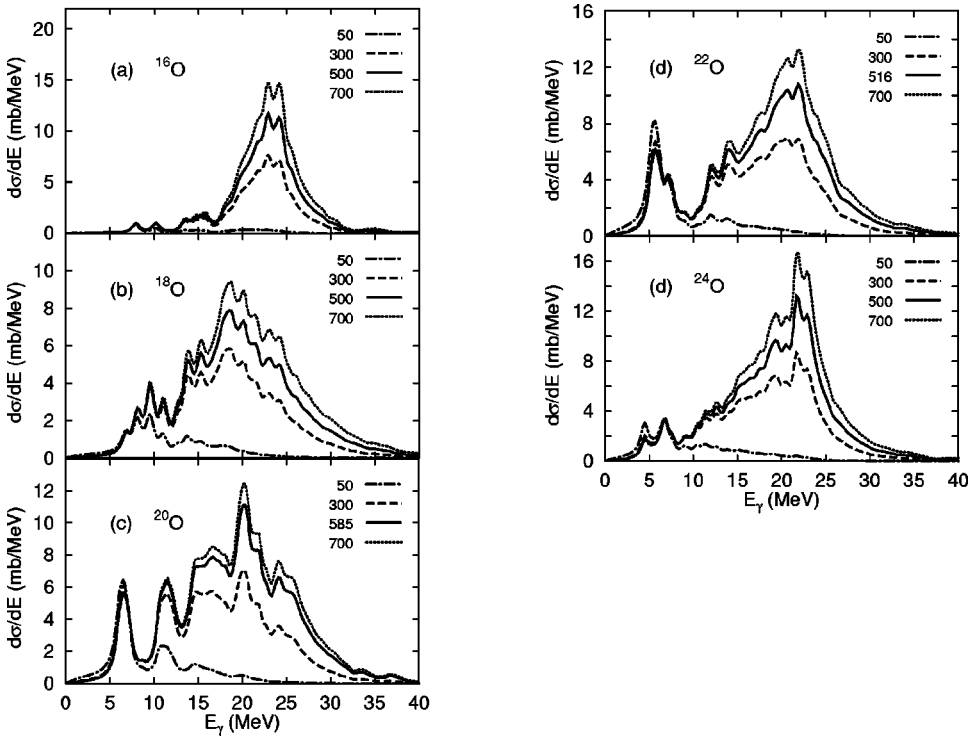

FIG. 8. Electromagnetic cross sections of $E1$ excitations within the PDM for oxygen isotopes on ^{208}Pb target. Different lines display results obtained at different projectile energies, whose values (in MeV/nucleon) are indicated in the panels.

It is known that different parametrizations of the Skyrme-type force lead to different single-particle energies. Among them, the SGII interaction, used in calculations in the present work, gives the most satisfactory results with respect to excitation energy, the width, and strength distribution for monopole and dipole compression modes in nuclei [16]. It is still worthwhile to see if changing the parametrization affects significantly the PDR. For this purpose, we have made a test using another parametrization of the Skyrme force, the SIII interaction, which uses a reasonable compromise between the deeply bound single-particle levels and those around the Fermi surface for over 200 open-shell nuclei [24]. We found that in order to reproduce the GDR's in oxygen isotopes at the same location and with a similar width as in the case using SGII interaction, the parameter f_1 must be reduced to 0.6595 MeV. The results obtained for the photoabsorption and EM cross sections in $^{18-24}$O are displayed in Figs. 10 and 11, respectively. These figures show that the use of single-particle energies generated by SIII interaction affects slightly the GDR shape, but the qualitative picture of the

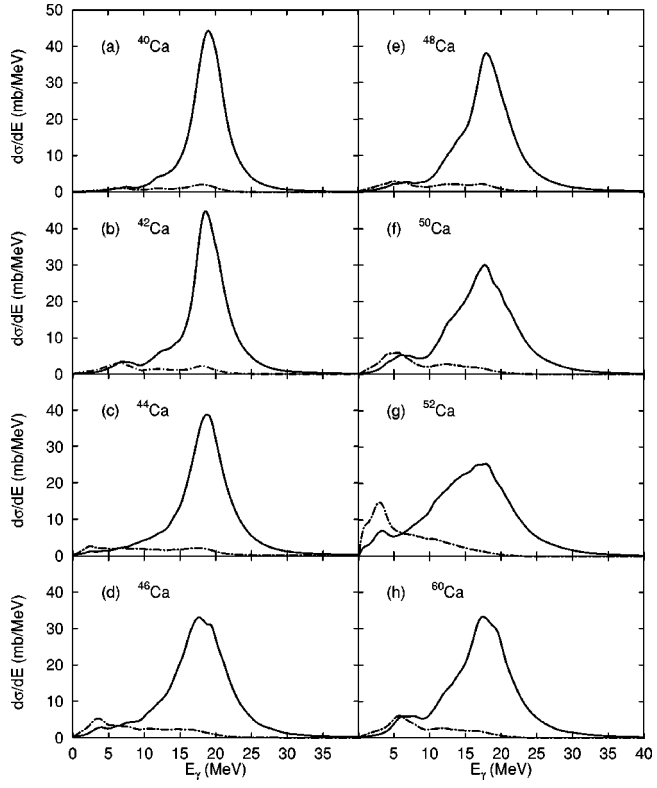

FIG. 9. Electromagnetic cross sections of $E1$ excitations within PDM for calcium isotopes on a ^{208}Pb target at 500 MeV/nucleon (solid lines) and 50 MeV/nucleon (dash-dotted lines).

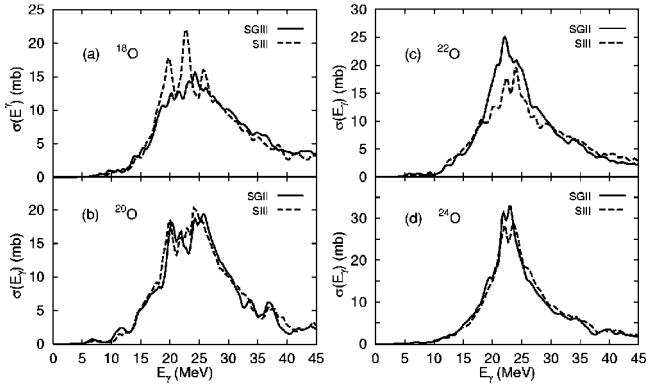

FIG. 10. Photoabsorption cross section within PDM for $^{18-24}$O. Solid lines are results obtained using single-particle energies generated by the SGII interaction (from Fig. 2), while dashed lines are those obtained using the SIII interaction.

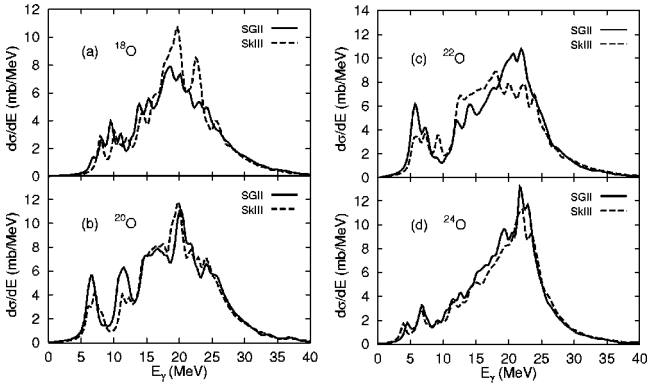

FIG. 11. Electromagnetic cross sections of $E1$ excitations within the PDM for $^{18-24}$O on ^{208}Pb target. Solid lines are results from Fig. 8, which are obtained using single-particle energies generated by the SGII interaction at the beam energy equal to 500 MeV/nucleon in (a) and (d), 585 MeV/nucleon in (b), and 516 MeV/nucleon in (c). Dashed lines are corresponding results obtained using the SIII interaction.

PDR remains the same with a pronounced structure around 7 MeV in the EM differential cross sections for ^{20,22}O (Fig. 11).

IV. CONCLUSIONS

In this work the PDM has been developed further to include the superfluid pairing in a microscopic manner. This accounts for the behavior of the neutron levels around the Fermi surface in a natural way, avoiding the need of introducing an ad hoc increase of p-h–phonon coupling f_1 in this region. The formalism is then applied to a systematic study of the GDR and PDR, with emphasis on the latter, in two chains, oxygen and calcium, starting from the double closed-shell nuclei, ^{16}O, ^{40}Ca, and ^{48}Ca, toward their neutron-rich isotopes. For the sake of simplicity and clarity, the PDM uses a single parameter f_1 for all matrix elements of the p-h–phonon coupling. This has been demonstrated to be a rather efficient PDM in the description of GDR damping for heavy nuclei at zero as well as nonzero temperatures [8,9] as in this region of high level density the configuration mixing makes the effects of different matrix elements look nearly the same. In the extension of approximation toward the low-energy tail of GDR and to lighter nuclei, this simplicity may become less efficient because of the low-level density. Therefore, one of the main goals of this work is to test the validity of the PDM in this region. The analysis of numerical calculations in this paper shows that a consistent and quantitative description of the PDR and GDR is achieved using the same sets of PDM parameters, which have been selected to describe correctly the GDR in double-closed shell nuclei. The shapes of photoabsorption cross sections obtained within the PDM are in reasonable agreement with the experimental systematics for the GDR in double closed-shell nuclei ^{16}O and ^{40,48}Ca.

The results of calculations show that the change of the fraction of the $E1$ integrated strength in the region of the PDR as a function of mass number A with increasing N is in agreement with the recent experimental data at GSI [2], and does not follow the prediction by the simple CM. This confirms the authentic damping mechanism of giant resonances given by the PDM as the result of coupling between collective phonon and noncollective p-h configurations. The CM can be considered as a simplified approximation in this picture, when the GDR is highly collective so that the motion of neutron excess can be well separated.

The present paper also demonstrates that the EM differential cross section may serve as a better probe for the PDR as compared to the photoabsorption cross section because, in the former, the low-energy tail of GDR is enhanced due to the photon spectral function. The EM differential cross sections obtained within the PDM in this work show prominent PDR peaks below 15 MeV for ^{20,22}O, in agreement with experimental observation. A more precise comparison is expected to be carried out after the final analysis of the GSI data. Furthermore, it is shown in this work that, using low-energy RI beams at around 50–60 MeV/nucleon, one can observe clean and even enhanced PDR peaks without admixture with the GDR in the EM differential cross sections of neutron-rich nuclei.

ACKNOWLEDGMENT

N.D.D. thanks D. Beaumel (Orsay) for fruitful discussions.

[1] J.G. Woodworth *et al.*, Phys. Rev. C **19**, 1667 (1979).
[2] T. Aumann *et al.*, GSI Scientific Report No. 1999, 2000, p. 27.
[3] Y. Alhassid, M. Gai, and G.F. Bertsch, Phys. Rev. Lett. **49**, 1482 (1982).
[4] P.-G. Reinhard, Nucl. Phys. **A649**, 305c (1999).
[5] E.G. Lanza, Nucl. Phys. **A649**, 344c (1999).
[6] H. Sagawa and T. Suzuki, Phys. Rev. C **59**, 3116 (1999).
[7] N. Dinh Dang, T. Suzuki, and A. Arima, Phys. Rev. C **61**, 064304 (2000).
[8] N. Dinh Dang and A. Arima, Phys. Rev. Lett. **80**, 4145 (1998); Nucl. Phys. **A636**, 427 (1998).
[9] N. Dinh Dang, K. Tanabe, and A. Arima, Phys. Rev. C **58**, 3374 (1998); Nucl. Phys. **A645**, 536 (1999).
[10] A.V. Ignatyuk, *Statistical Properties of Excited Atomic Nuclei* (Energoatomizdat, Moscow, 1983).
[11] A. Bohr and B.R. Mottelson, *Nuclear Structure* (Benjamin, New York, 1969), Vol. 1, p. 170.
[12] D.N. Zubarev, Usp. Fiz. Nauk. **71**, 71 (1960) [Sov. Phys. Usp. **3**, 320 (1960)].
[13] N.N. Bogolyubov and S.V. Tyablikov, Dokl. Akad. Nauk (SSSR) **126**, 53 (1959) [Sov. Phys. Dokl. **4**, 589 (1959)].
[14] W.J. Llope and P. Braun-Muzinger, Phys. Rev. C **41**, 2644 (1990).
[15] I.A. Pshenichnov *et al.*, Phys. Rev. C **60**, 044901 (1999).
[16] N. Van Giai and H. Sagawa, Nucl. Phys. **A371**, 1 (1981).
[17] J. Ahrens *et al.*, Nucl. Phys. **A251**, 479 (1975).

[18] G.J. O'Keefe, M.N. Thompson, Y.I. Assafiri, R.E. Pywell, and K. Shoda, Nucl. Phys. **A649**, 239 (1987).
[19] P.F. Bortignon and R.A. Borglia, Nucl. Phys. **A371**, 405 (1981).
[20] S. Nishizaki and J. Wambach, Phys. Lett. B **349**, 7 (1995).
[21] S. Kamerdzhiev, J. Speth, and G. Tertychny, Nucl. Phys. **A624**, 328 (1997).
[22] T. Hartmann, J. Enders, P. Mohr, K. Vogt, S. Volz, and A. Zilges, Phys. Rev. Lett. **85**, 274 (2000).
[23] S. Mizutori, J. Dobaczewski, G.A. Lalazissis, W. Nazarewicz, and P.-G. Reinhard, Phys. Rev. C **61**, 044326 (2000).
[24] M. Beiner, H. Flocard, N. Van Giai, and P. Quentin, Nucl. Phys. **A238**, 29 (1975).